# $^{14}C(\pi^+,\pi^-)^{14}O$ reaction between 19 and 80 MeV

M. J. Leitch, H. W. Baer, R. L. Burman, and C. L. Morris
*Los Alamos National Laboratory, Los Alamos, New Mexico 87545*

J. N. Knudson* and J. R. Comfort
*Arizona State University, Tempe, Arizona 85287*

D. H. Wright†
*Virginia Polytechnic Institute and State University, Blacksburg, Virginia 24061*

R. Gilman‡
*University of Pennsylvania, Philadelphia, Pennsylvania 19104*

S. H. Rokni§
*Utah State University, Logan, Utah 84322*

E. Piasetzky and Z. Weinfeld
*Raymond and Beverly Sackler Faculty of Exact Science, Tel Aviv University, Ramat Aviv, Israel*

W. R. Gibbs and W. B. Kaufmann
*Theoretical Division, Los Alamos National Laboratory, Los Alamos, New Mexico 87545*
*and Arizona State University, Tempe, Arizona 85287*
(Received 19 December 1988)

Cross-section measurements are reported for the $^{14}C(\pi^+,\pi^-)^{14}O$ reaction to the double isobaric analog state and for nonanalog states at 5 to 10 MeV excitation. The extrapolated zero-degree cross sections are $2.3\pm0.5$, $3.7\pm0.4$, $2.2\pm0.3$, and $0.9\pm0.3$ $\mu$b/sr at 19.0, 29.1, 64.4, and 79.5 MeV, respectively. The nonanalog-state cross sections are found to rise sharply with increasing beam energy above 50 MeV, in contrast to those of the double isobaric analog state transition. Calculations with a phenomenological isospin-dependent optical potential must include an isotensor term, which accounts for transitions through nonanalog intermediate states or other short-range correlations, in order to describe the energy and angular trends of the data. Microscopic calculations in the second-order distorted-wave impulse approximation fail to reproduce the cross sections near 50 MeV unless the effects of short-range correlations beyond those contained in the model are incorporated.

## I. INTRODUCTION

The pion double-charge-exchange (DCX) reaction is of fundamental interest due to its potential for probing nucleon-nucleon (*NN*) correlations in nuclei. Reactions at low energies are especially important because of the increased penetration of the pion into the interior of the nucleus. At energies near the $P_{33}$ resonance the pion interacts at about the 10% density point of the nuclear medium, while at low energy it penetrates more fully into the nuclear volume.[1] There is also a deep forward-angle minimum near 50 MeV in the cross section for single-charge-exchange (SCX) reactions to the isobaric analog state[2,3] (IAS) that inhibits the double-forward sequential SCX scattering through the intermediate analog state. Thus, processes such as scattering through nonanalog intermediate states[4] and mechanisms involving short-range nucleon pairs[5–7] may be more readily observable. Recent measurements[8–10] of the double isobaric analog state (DIAS) transition for $^{14}C$, $^{18}O$, and $^{26}Mg$ at 50 MeV showed that the forward-angle cross sections are large, of order 4 $\mu$b/sr at 0°, and that the angular distributions are forward peaked. Several theoretical studies[5–7] have attributed these features to the significant role of short-range *NN* correlations, such as those contained in six-quark clusters.

We present here a detailed study of the energy dependence of the forward-angle DIAS cross sections for $^{14}C$ in the interval 19–80 MeV. Since $^{14}C$ is the lightest $T=1$ nucleus, it provides the simplest case for the theoretical predictions of the cross section. Experimentally, $^{14}C$ is well suited since the DIAS transition to the ground state of $^{14}O$ is separated by 5.2 MeV from the first excited state. Therefore, the $^{14}C$ cross sections are typically the most accurate and can be measured for nearly any angle and energy. Along with the extensive single-charge-exchange data (Ref. 3), they form an exceptionally complete data set that puts strong constraints on the theoretical models. A large body of DCX data on $^{14}C$ already exists at and above 80 MeV.[11] However, only one previous

 

angular distribution at 49 MeV exists in the low-energy region.[8,9]

## II. EXPERIMENT

The measurements were carried out with the Clamshell spectrometer at the Low-Energy Pion channel[12] of the Clinton P. Anderson Meson Physics Facility (LAMPF). Pion beams with momentum bites of 0.25–4 % (full width) and fluxes between $5\times10^6$ and $3\times10^7$ pions/sec were used. The runs at small angles required lower beam fluxes in order to keep the singles rates in the scintillator at the entrance to the spectrometer magnet at tolerable levels. At higher energies the inherently greater beam fluxes were reduced by closing the momentum slits of the channel. Since the first excited state in the residual $^{14}O$ nucleus is at 5.2 MeV, the large momentum bites of 3–4 % used at 29 MeV still allowed clean separation of the ground state from higher-lying states.

The $^{14}C$ target consisted of two powder-filled-thin-walled copper cells ($5\times5\times0.6$ cm$^3$). The powder was 77% $^{14}C$, 14% $^{12}C$, and 9% impurities by weight. The two cells together had a total $^{14}C$ target thickness of $0.29\pm0.02$ g/cm$^2$, and a total copper wall thickness of 0.18 g/cm$^2$. Empty copper cell runs were taken but yielded almost no scattered pions in the region of the DIAS.

The Clamshell spectrometer is a single magnetic dipole spectrometer with nonparallel pole faces, a solid angle of about 35 msr, an average flight path of particles passing through it of about 2 m, and can achieve a resolution of a few hundred keV under the best conditions. A small scintillator at the entrance to the dipole and two large scintillators near the focal plane provide the trigger for the system. Two $x$-$y$ delay-line drift chambers[13] located in front of the large scintillators provide the position and angle of each particle track for both the momentum and the transverse directions. For the 19-MeV data and for the 29-MeV data at 130 deg, an additional stopping scintillator was located behind the second large scintillator; it helped in identifying pions by measuring their total stop-

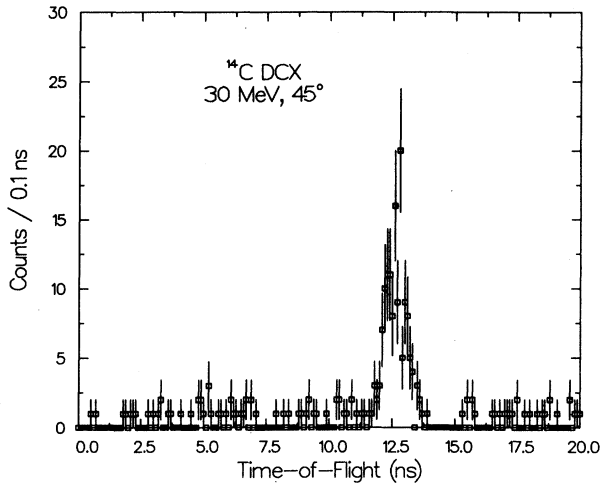


FIG. 1. Time-of-flight spectrum for double-charge exchange on $^{14}C$ at 30 MeV and 45°. The peak corresponds to pions from the DCX reaction and the flat background is due to random coincidences between the front and rear scintillators.

TABLE I. Measured differential cross sections for the reaction $^{14}C(\pi^+,\pi^-)^{14}O$ for the DIAS transition and for nonanalog states.

| $T_\pi$ (MeV) | $\theta_{c.m.}$ | $d\sigma/d\Omega_{c.m.}^{DIAS}$ ($\mu$b/sr) | $d\sigma/d\Omega_{c.m.}^{NA\,b}$ ($\mu$b/sr) |
|---|---|---|---|
| 19.0 | 40.5 | 2.0±0.4 | |
| 29.1 | 20.3 | 3.19±0.44 | |
| | 45.6 | 3.62±0.49 | |
| | 90.8 | 1.59±0.24 | |
| | 130.6 | 0.93±0.21 | |
| 49.2[a] | 20.3 | 3.26±0.23 | |
| | 30.4 | 3.04±0.22 | |
| | 40.5 | 2.48±0.18 | 0.62±0.17 |
| | 50.6 | 1.97±0.18 | |
| | 60.7 | 1.56±0.12 | |
| | 70.8 | 1.32±0.32 | |
| | 80.8 | 0.88±0.11 | |
| | 90.8 | 0.73±0.07 | |
| | 130.6 | 0.65±0.10 | |
| 64.4 | 20.3 | 1.70±0.24 | |
| | 40.6 | 1.28±0.12 | 1.78±0.18 |
| | 60.8 | 0.58±0.08 | 1.68±0.18 |
| | 90.9 | 0.26±0.04 | 2.36±0.22 |
| 79.5 | 25.4 | 0.44±0.12 | 1.43±0.39 |

[a]From Ref. 8.

[b]Summed cross section for states at 5–10 MeV excitation in $^{14}O$.

ping energy.

The final particle identification for the DCX reaction was obtained from a time-of-flight measurement between the small front scintillator and the large focal-plane scintillators. Since the length of the particle flight path and the particle momentum each vary by a large amount over the length of the focal plane, about 40% and 50%, respectively, corrections for both of these were made. The measured time-of-flight was corrected to the central-ray value by applying a polynomial in position and angle

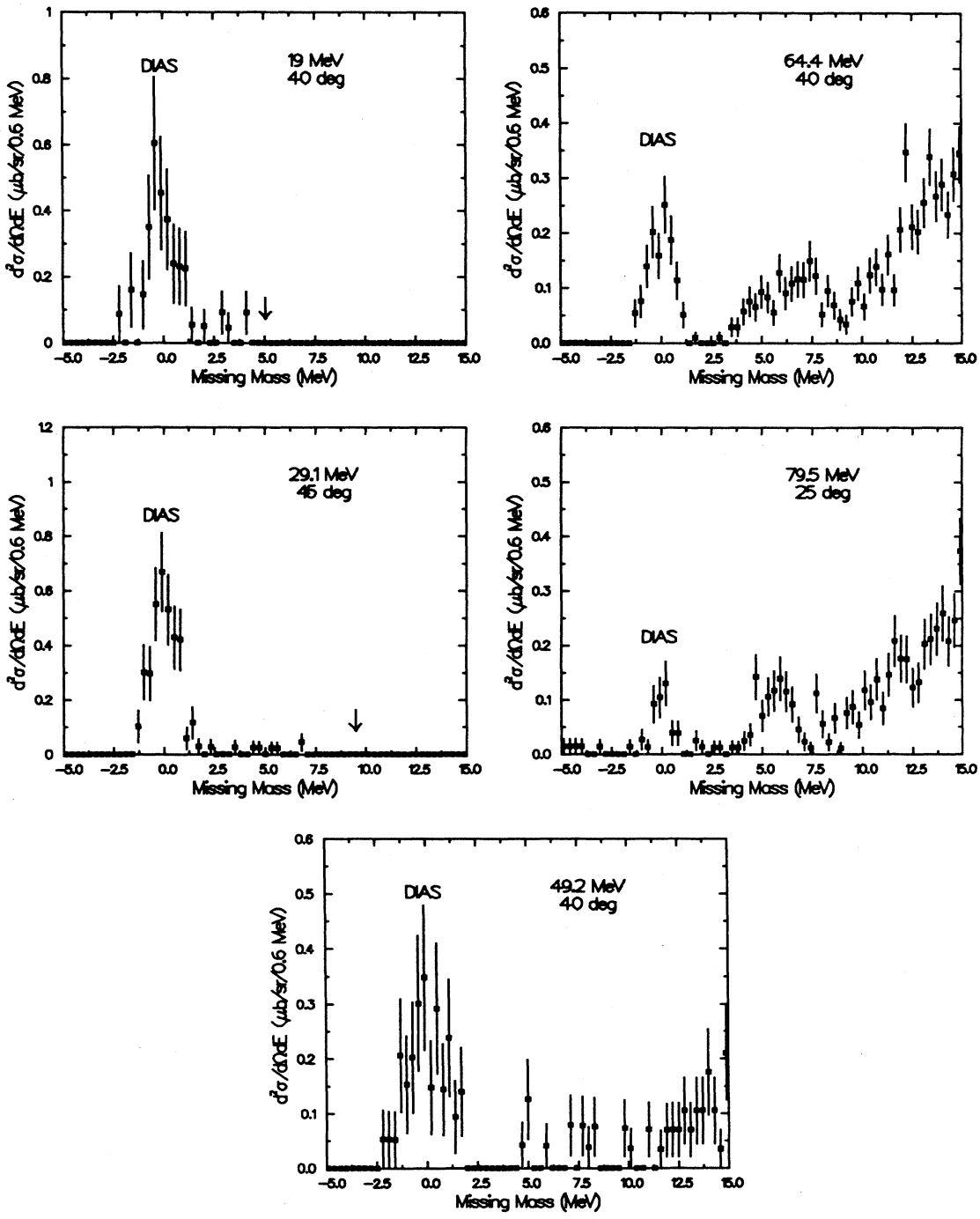


FIG. 2. Missing mass spectra for the reaction $^{14}C(\pi^+,\pi^-)^{14}O$ at forward angles for five different energies. The low-energy acceptance cutoff for the 19- and 29.1-MeV spectra are shown by the arrows.

along the momentum direction. A typical corrected time-of-flight spectrum is shown in Fig. 1; it has a resolution of about 1 ns full width at half maximum (FWHM). Most of the electrons that would have otherwise appeared in these spectra have already been removed by a requirement that the pulse heights in the two focal-plane scintillators exceed a minimum value. The momentum of the scattered particle was determined by using a polynomial in position and angle along the momentum direction as measured by the two multiwire proportional chambers.

To identify unambiguously the expected location of the DIAS peak for the $^{14}C$ DCX reaction and to provide the normalization, we took companion runs of $\pi^+$ elastic scattering on $^{12}C$. The known cross sections for $^{12}C$ elastic scattering[14] were used, with suitable interpolation to the exact energies at the center of our target.

The relative pion fluxes between the elastic-scattering and the DCX measurements were monitored by integrating the primary proton beam current which passed through a torroidal current monitor placed just upstream of the pion-production target. The stability of this method was confirmed by elastic-scattering measurements taken before and after the DCX measurements at each energy and angle.

The nonanalog transitions for 30-MeV incident pions produced such low-energy pions ($\simeq$12 MeV incident on the focal plane) that they nearly stopped in the first focal-plane scintillator. Since the second focal-plane scintillator was required in the system trigger, many of these probably did not trigger and were lost. Thus, nonanalog cross sections could not be reliably extracted from the data at 30 MeV and below.

The resolution obtained in these measurements varied with energy and angle but was usually dominated by the effect of the large momentum bite in the incident pion beam. For most of the measurements the energy resolution was between 1.0 and 1.5 MeV (FWHM), except for the 29-MeV measurement at 130° which had a resolution of about 3.5 MeV.

Spectra obtained at each energy are shown in Fig. 2. The DIAS peak is clearly visible and is well separated from the first excited state at 5.2 MeV. The yields in the DIAS peaks and in the nonanalog region of less than 10 MeV excitation were obtained by summing the counts in the relevant part of the spectra and, where appropriate, subtracting a nonphysical background whose level was determined by the number of counts in the region above the energy of the DIAS peak. The resulting cross sections and their uncertainties are presented in Table I. The uncertainties are dominated by the statistics of each measurement, with an additional contribution from the uncertainty in the elastic cross sections used for normalization. A further contribution of ±10% to the absolute normalization comes from the uncertainty in the target thicknesses.

## III. RESULTS AND COMPARISONS WITH OTHER DATA

### A. Angular distributions and extrapolations to 0°

The DIAS cross sections as measured in this work at 29.1, 64.4, and 79.5 MeV, and as previously measured[7] at 49.2 MeV are shown in Fig. 3. Also shown is the 5° cross section at 80 MeV previously measured at the EPICS beam channel.[11] The shapes of the angular distributions, as established by these data, exhibit a gradual transition from near isotropy at 29.1 MeV to forward peaking at high energies.

Since it has been of interest to compare experimental 0° excitation functions with theoretical calculations, we used extrapolation procedures to estimate the 0° cross sections. For the data at 29.1, 49.2, and 64.4 MeV, we fitted the simple function

$$d\sigma/d\Omega = Ae^{\lambda(\cos\theta-1)}+B\ ,$$

where $\theta$ is the center-of-mass scattering angle and $A$, $\lambda$, and $B$ are parameters.[8] The fitted curves, as shown in Fig. 3, provide good descriptions of the data. Since there are insufficient data at 19.0 and 79.5 MeV for this method, the extrapolated 0° cross sections at these energies were obtained by normalizing the theoretical angular distributions that are discussed in Sec. IV to the available data points. The 5° cross section at 80 MeV provides a strong constraint on the corresponding extrapolated 0° cross section. The theoretical model provides a nearly isotropic angular distribution at 19 MeV and the extrapolated 0° cross section is only about 15% greater than the 40° datum. To the extent that other reaction models have similar angular distributions, comparisons may be made with the 0° cross section.

The extrapolated 0° cross sections at all five energies are given in Table II. The angle-integrated cross sections obtained with the above functional form are 23.2±4.3, 15.3±1.6, and 6.3±1.9 $\mu$b at energies of 29.1, 49.2, and 64.4 MeV, respectively.

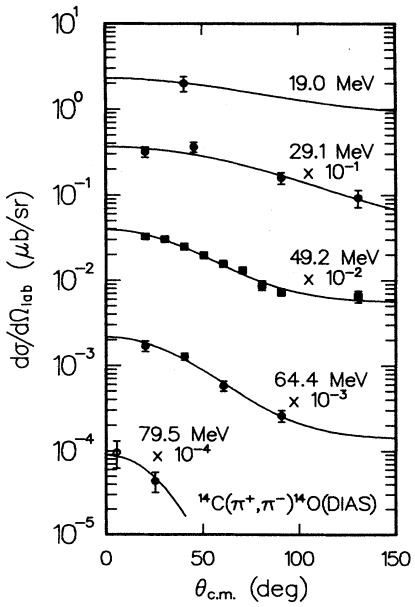


FIG. 3. Angular distributions for the reaction $^{14}C(\pi^+,\pi^-)^{14}O$ (DIAS) at five energies. The data at 49 MeV are from Ref. 8, and the 5° point at 80 MeV is from Ref. 11. The curves are fits to the data as described in the text.

TABLE II. Extrapolated 0° differential cross sections for the reaction $^{14}C(\pi^+,\pi^-)^{14}O$ to the double isobaric analog state. The extrapolation procedures are defined in Sec. III A.

| $T_\pi$ (MeV) | $d\sigma/d\Omega_{c.m.}^{DIAS}$ ($\mu$b/sr) |
|---|---|
| 19.0 | 2.3±0.5 |
| 29.1 | 3.7±0.4 |
| 49.2[a] | 3.9±0.5 |
| 64.4 | 2.2±0.3 |
| 79.5 | 0.9±0.3 |

[a]From Ref. 8.

### B. Nonanalog transitions

An interesting aspect of DCX reactions at low energies exhibited by the present data is the rapid increase with increasing energy of the transition strength to the nonanalog states in the 5–10-MeV region of excitation in $^{14}O$. This feature can be seen in the spectra of Fig. 2, which have been corrected for the energy dependence of the spectrometer acceptance function. To quantify this trend, we summed the counts between 5 and 10 MeV and obtained cross sections for these yields. The values are given in Table I. This analysis could only be done for the data at 49.2, 64.4, and 79.5 MeV where the spectrometer acceptance was reliably known for the full energy interval. For the 19- and 29.1-MeV data, the acceptance function falls off rapidly between 8 and 10 MeV.

From the cross sections given in Table I, we see that the DIAS and nonanalog-state cross sections have contrasting energy dependence. For example, the 40.5° DIAS cross sections are 2.5 and 1.3 $\mu$b/sr at 49.2 and 64.4 MeV, respectively, while the nonanalog-state values are 0.6 and 1.7 $\mu$b/sr, respectively. This result is puzzling in view of recent theoretical studies concerning the role of nonanalog intermediate states in DIAS transitions.[7] These studies indicate that the contribution of nonanalog intermediate states is much larger at 50 MeV than at higher incident energies. Here we see that the population of nonanalog final states (in $^{14}O$) is relatively small at 50 MeV compared to higher energies.

### C. Forward-angle excitation functions

The full forward-angle excitation functions as they are now known for the DIAS transitions on $^{14}C$ and $^{18}O$ are shown in Fig. 4. The present study establishes the shape of this function between 19 and 80 MeV for $^{14}C$. For these energies the cross sections shown are extrapolated 0° cross sections, as discussed above. For higher energies, the measured 5° cross sections are shown. The new feature determined here is the increase in the cross section between 19 and 30 MeV, a feature that the calculations presented below are not able to reproduce.

### D. Comparisons to DCX reactions on $^{18}O$ and $^{12}C$

The forward-angle excitation function for the DIAS transition on $^{18}O$ is shown in Fig. 4 and that for the nonanalog ground-state transition on $^{12}C$ is shown in Fig. 5. The $^{12}C$ excitation function exhibits the resonance shape found for all $T=0$ nuclei, with a peak cross section near 180 MeV. This feature is not observed for the $^{14}C$ DIAS transition, but is for both $^{16}O$ and $^{18}O$. The reason for this difference between the isotope pairs $^{12,14}C$ and $^{16,18}O$ is not understood.

The rise in the $^{12}C(\pi^+,\pi^-)$ cross section at low energies follows the trend of the $^{14}C$ DIAS cross section. The fact that the $^{12}C$ and $^{14}C$ cross sections both rise forces one to seek an explanation common to both types of transitions. One common factor is the increased pion penetration at lower energies, and it is likely responsible for some increase in the cross sections. A second factor, as given by the theoretical analyses discussed below, is the enhanced scattering amplitude through nonanalog intermediate states at incident energies near 50 MeV. Since $^{12}C$ has no IAS, nonanalog amplitudes are the only types available.

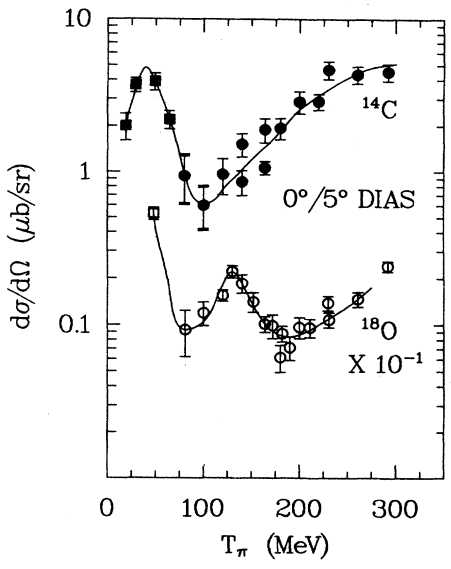


FIG. 4. Excitation functions for 0°/5° pion double-charge-exchange reactions to the DIAS for $^{14}C$ and $^{18}O$. The curves are to guide the eye. The data at 19.0, 29.1, 64.4, and 79.5 MeV for $^{14}C$ are from this work. The other data are from Refs. 8, 10, 11, and 15.

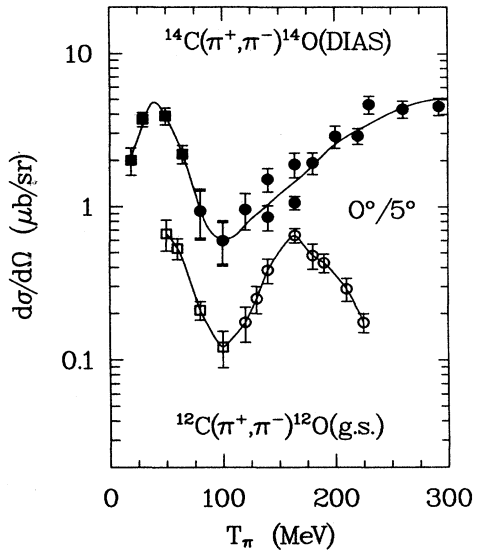


FIG. 5. Excitation functions for 0°/5° pion double-charge exchange to the DIAS for $^{14}C$ compared to that for the nonanalog ground-state transition for $^{12}C$ (from Ref. 16). The curves are to guide the eye.

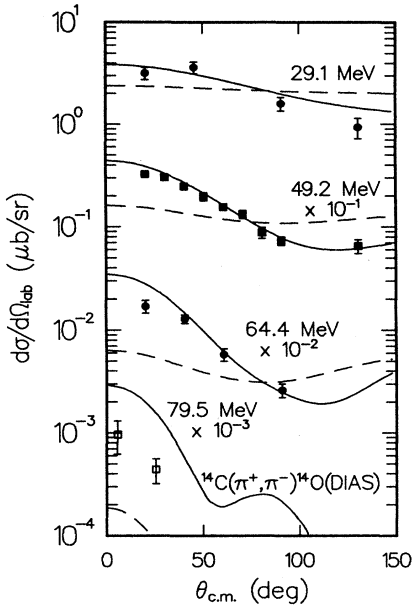


FIG. 6. Measured angular distributions for the reaction $^{14}C(\pi^+,\pi^-)^{14}O$ (DIAS) compared with phenomenological isospin-dependent optical-model calculations with (solid) and without (dashed) isotensor terms as described in Sec. IV A.

## IV. THEORETICAL CALCULATIONS AND DISCUSSION

The data obtained in this experiment will be compared with calculations obtained from two theoretical models. First, we show results from a phenomenological isospin-dependent optical-potential calculation which exhibit the need for terms that go beyond the isoscalar and isovector strengths determined from known elastic and single-charge-exchange scattering. Then we use a second-order distorted-wave impulse approximation (DWIA) to specifically investigate the dynamics and shell-model dependence of the DCX reaction on $^{14}C$. These calculations demonstrate the importance of nonanalog intermediate states as well as the significant role of nucleon-nucleon correlations

### A. Phenomenological isospin-dependent optical-potential calculations

The phenomenological isospin-dependent optical-model program, PIESDEX of Siciliano and Johnson,[1] was used to calculate DCX cross sections. One set of calculations is based upon fits, without a phenomenological isotensor term, to pion elastic and single-charge-exchange data for $^{14}C$. A second set of calculations includes a phenomenological isotensor term that was adjusted to give good agreement with the 50-MeV DCX data. This optical-model program solves the Klein-Gordon equation on channels of good total isospin, then projects onto the physical scattering channels. It is essentially an extension of the Michigan State University (MSU) approach used for elastic scattering[17] with second-order isovector and isotensor terms added. In the calculations shown here we have followed Ref. 1, where the isoscalar parameters were taken from the MSU potential and the one isovector and one isotensor parameters were chosen to give good agreement with the 50-MeV $^{14}C$ SCX and DCX data. These values are the same as those used in Refs. 1 and 18. Coulomb effects are not included in the calculation of double-charge exchange although they are included in comparisons with elastic scattering data.

The resulting calculations are shown in Fig. 6 where the dotted curve is with the isotensor strength set to zero (all sequential DCX through the analog intermediate state), and the solid curve is the full calculation. The calculations without the isotensor strength have a shape that is too flat compared to the data, presumably because they leave out important effects due to nonanalog intermediate states or related short-range effects. With the energy-independent isotensor term, the full calculations approach the data at energies from 29.1 to 64.4 MeV.

### B. Microscopic DWIA calculations

#### *1. The reaction model*

A theoretical model has been developed that provides a microscopic treatment of pion elastic-scattering and charge-exchange reactions from nuclei.[6,19] In this model, the free pion-nucleon amplitudes are used to construct optical potentials that are then used in impulse approximation calculations of the reaction. The transition operators describing the charge exchange[20] are consistent with the pion-nucleon amplitudes that are used to construct the optical potential.

The DCX process is assumed to proceed through two single-charge-exchange steps on the valence nucleons. The transition amplitude is described schematically as

$$A = \sum_{m \neq n} \langle \Phi_f \psi_{\vec{k}'}^{(-)} | f_m \frac{1}{p^2 + 2\omega(H_N + U) - k^2 - i\epsilon} f_n | \Phi_i \psi_{\vec{k}}^{(+)} \rangle \ . \quad (1)$$

In this expression $f_m$ is the off-shell pion-nucleon charge-exchange operator on the valence neutron $m$, $\Phi$ is the nuclear shell-model wave function (angular momentum couplings implicit), $\psi^+$ is the pion distorted wave corresponding to incident $\pi^+$, and $\psi^-$ is its time- and charge-reversed partner, $\omega$ is the reduced pion-nucleus energy, $H_N$ is the total nuclear hamiltonian, and $p$ and $U$ are the pion-nucleus relative momentum operator and optical potential.

The pion-nucleus propagator is evaluated as follows: The relatively low-lying intermediate nuclear states are assumed to be the most important so that the nuclear Hamiltonian may be replaced by an effective nuclear energy which is close to the ground state. This procedure removes explicit dynamical dependence on the intermediate nuclear states and is referred to as the closure approximation. It is assumed that the optical potential for pions scattering on the intermediate (possibly excited) state is the same as if the nucleus were in its ground state. The propagation of the pions is described by a finite-range nonlocal optical potential which employs large matrices in coordinate space to express the pion-nucleus potential. The solution to this linear system of equations (with the inclusion of the Coulomb potential and appropriate boundary conditions) gives the pion wave functions. In the same manner the inversion of the matrix describing the system (again with appropriate boundary conditions) provides the Green's function necessary for the evaluation of Eq. (1).

The two single-exchange amplitudes are treated as operators on the pion-nucleus relative momenta. The off-shell behavior of these amplitudes is described by Yamaguichi monopole form factors with a range of 700 MeV/$c$, while a range of 300 MeV/$c$ was used for the construction of the optical potential. Double-spin-flip amplitudes, whose significant role has been noted by Bleszynski and Glauber,[7] have been included.

In order to include a correction for pion true absorption, a pure imaginary term was added to the optical potential of the form $W\rho^2$, where $\rho$ is the nuclear density (nucleons per fm$^3$). The value of $W$ was determined at each energy for $^{12}$C by comparison of the predicted true-absorption cross section with the experimental values of Ashery *et al.* and Navon *et al.*[21] or with Nakai *et al.*[22] Since Ref. 21 contains data on $^{12}$C but very little low-energy data, while Ref. 22 has a fairly extensive set of low-energy points but only on medium-weight and heavy nuclei, we have extracted values of $W$ as a function of energy from both of these two data sets. Since there are discrepancies between the data sets where they do overlap (e.g., $^{27}$Al), and since the manner in which the $W$ is inferred from the true-absorption data is not unique,[19] there is considerable uncertainty in the values obtained. The range of values that are permitted by these procedures is indicated in Fig. 7. No $p$-wave term was included so that all the pion removal has been lumped into an $s$-wave term. However, the resonant nature of the process is clearly seen as the steep rise with energy. The normalization of $W$ is such that

$$2\omega V_{\text{abs}} = -iW\rho^2(r) \ , \quad (2)$$

where $\rho(r)$ is normalized such that $\int_0^\infty r^2 dr\, \rho(r) = 1$ and $W(A) = W_0 A^2$, where $A$ is the nuclear mass number and $W_0$ is independent of $A$. To use the data of Ref. 22, the values of $W$ for $^{12}$C are obtained by scaling those of $^{27}$Al by $(\frac{12}{27})^2$.

The final DWIA calculations used values of $W$ that were near the low end of the range shown in Fig. 7, corresponding to the data of Ref. 21. Since the incident $\pi^+$ and the outgoing $\pi^-$ have roughly the same kinetic energy in the nuclear interior after allowance is made for the Coulomb barrier, it is reasonable to use the $\pi^+$ energy for evaluating $W$ for both the incoming and outgoing pions. Since closure is used on the intermediate states, the appropriate $\pi^0$ energy is not well defined. Hence the same value of $W$ (that for the $\pi^+$) was used throughout the calculation.

The nuclear isovector transition amplitudes were obtained from the shell-model calculations of Cohen and Kurath.[23] The $p$-shell radial wave functions were obtained as solutions to the Schrödinger equation with a Woods-Saxon potential whose well depth was chosen to reproduce the experimental separation energies for the initial $^{14}$C (neutron) and final $^{14}$O (proton) nuclear states.

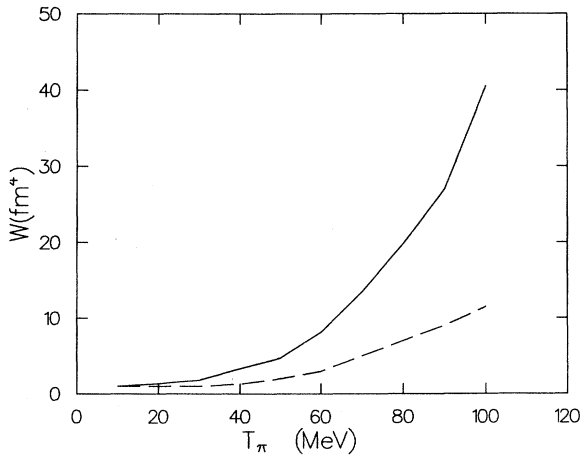


FIG. 7. Values of the coefficient $W$ of $\rho^2$ which represents pion true absorption. The solid curve is derived from the absorption data of Ref. 22 and the dashed curve from the data of Ref. 21.

### 2. *DWIA model results*

The results of the microscopic DWIA calculations for the angular distributions are shown as solid curves in Fig. 8. The short-dashed curves are the results of plane-wave calculations with the same parameters. The model predicts a gradual forward peaking of the angular distribution shape as the energy is raised from 10 to 80 MeV, a trend that is evident in the data. Although the cross-section scale is approximately reproduced at the two ends of the energy range, the calculations fall substantially below the data in the region between 30 and 60 MeV. The plane-wave calculations are much less successful in reproducing the trends with either energy or angle.

The effects of distortion are found to be very significant throughout the entire energy range. This conclusion is in agreement with the results of Kobayashi and Karapiperis,[4] but is at odds with that of Bleszynsky and Glauber,[7] who claim a much smaller effect at 50 MeV. Indeed, the distortion of the intermediate $\pi^0$ is found to be very important, especially in the 30–60-MeV region. Turning off the $\pi^0$ distortions reduces the cross sections

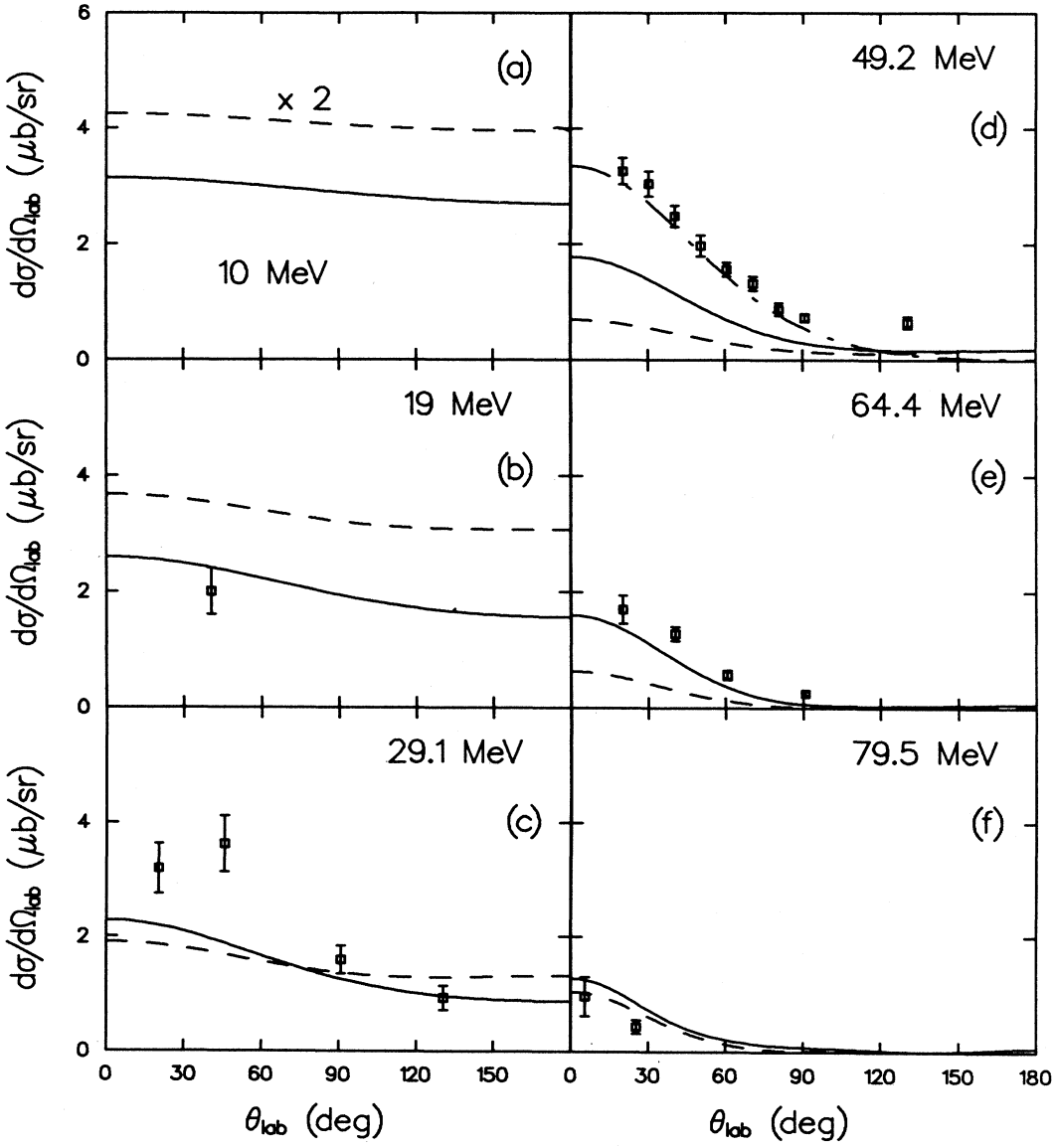


FIG. 8. Angular distributions for the reaction $^{14}C(\pi^+,\pi^-)^{14}O$ (DIAS) at 10, 19, 29.1, 49.2, 64.4, and 79.5 MeV. The curves shown are obtained from full microscopic DWIA calculations (solid curves) and plane-wave calculations (short-dashed curves). The dash-dotted curve at 49.2 MeV represents a DWIA calculation with only a $^1S_0$ amplitude.

even further in this intermediate region. The effects of such distortions are treated in only an approximate "on-shell" manner in Ref. 7.

The 0° cross sections are shown as a function of energy in Fig. 9. The solid curve again represents the full calculation while the long-dashed curve is obtained from calculations in which the double-spin-flip term is excluded. This double-spin-flip term has a relatively small effect (~20%) at low energies, but makes differences of as much as a factor of 3 to 4 near 80 MeV. Increasing the pion absorption will produce worse agreement with the 0° excitation function in the region between 30 and 60 MeV. It appears, therefore, that important dynamical or structure effects are not being taken into account in this energy region.

A clue as to the cause of the disagreements between the model and the data near 50 MeV is indicated by the dash-dotted curve in Fig. 9. The corresponding angular distribution at 49.2 MeV is shown as the dash-dotted curve in Fig. 8. These curves result from a DWIA calculation with only a $^1S_0$ amplitude. This term corresponds to the maximum possible correlation between two $p$-shell nucleons.[6] This correlation is proportional to the square of the cosine of the relative angle between the valence neutrons and leads to a high probability of close $NN$ encounters, strongly enhancing the DCX process. Although this calculation is not intended to represent a proper solution to the problem, it suggests that one may need to look for additional terms in the model that will enhance the correlations such as mixed-shell wave functions from an extended shell-model basis or meson-exchange contributions.[24]

More insight into both distortions and the $NN$ separation may be obtained if we divide the DCX transition amplitude into its monopole ($A$) and quadrupole ($B$) components, as was done in Ref. 24. The cross section is then equal to $(k'/k)|A+XB|^2$, where $X$ depends on the shell-model configuration ($X=1.21$ for the Cohen and Kurath amplitudes, and $X=2.0$ for the $^1S_0$ amplitude) and $k$ ($k'$) is the initial (final) momentum. In this language, the $A$ amplitude corresponds approximately to sequential SCX reactions through the intermediate analog state, while the $B$ amplitude corresponds approximately to transitions though nonanalog intermediate states. In the plane-wave limit, the $A$ term is not sensitive to two-nucleon correla-

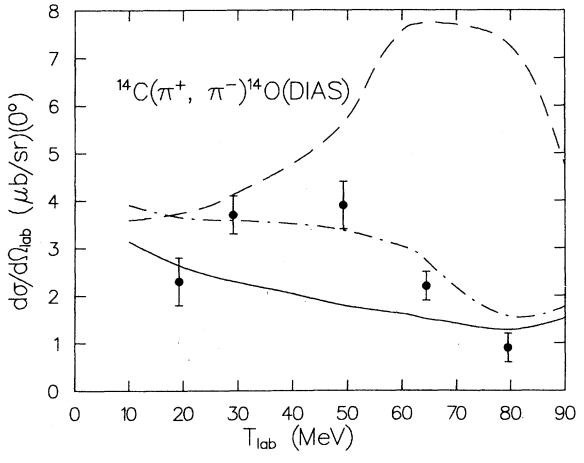


FIG. 9. Excitation functions for the reaction $^{14}C(\pi^+,\pi^-)^{14}O$ (DIAS) at 0°. The curves shown are obtained from full microscopic DWIA calculations (solid curve), DWIA calculations with the double-spin-flip amplitudes excluded (long-dashed curve), and DWIA calculations with only a $^1S_0$ amplitude (dash-dotted curve).

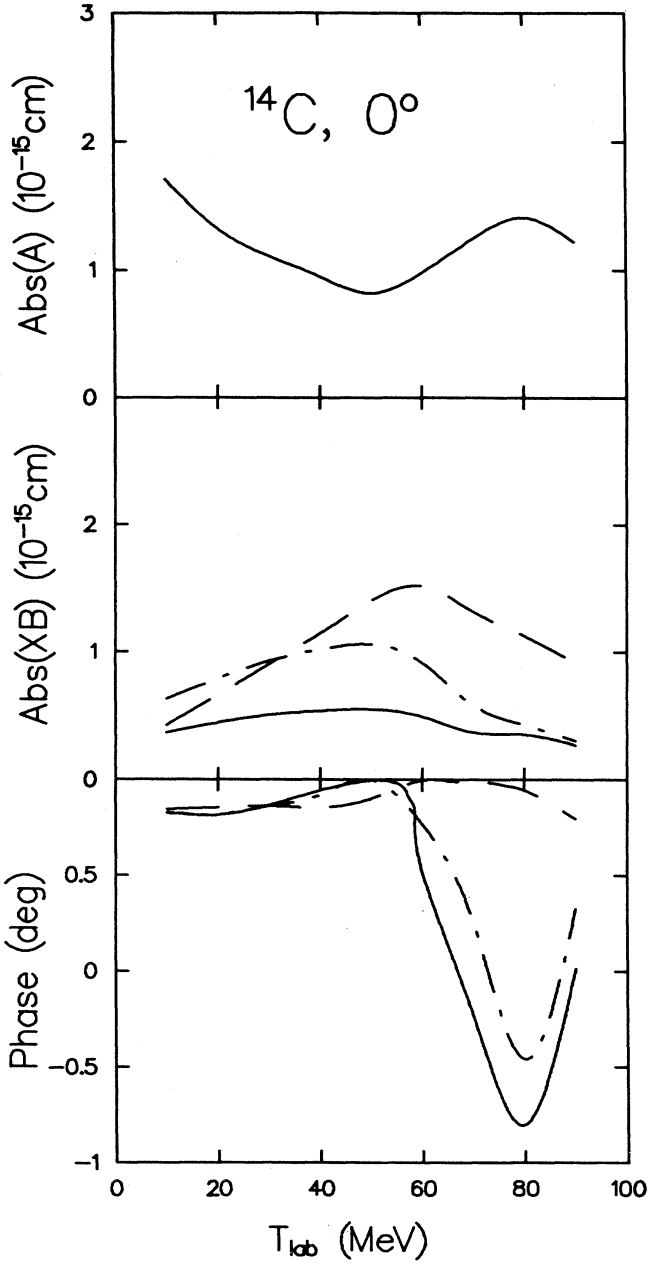


FIG. 10. The magnitudes of $A$, $XB$, and their relative phase versus incident pion energy. The meaning of the curves is the same as for Fig. 9.

tions and is generally long range, of the order of 2–4 fm.[7,24,25] The $B$ term contains the principal effects of the correlations and is of much shorter range, typically about 1 fm.[6,7,24]

The energy dependences of the $A$ and $B$ amplitudes and the phase between them, as computed from the theoretical model used here, are shown in Fig. 10. Again, the solid curve represents the DWIA calculation, the short-dashed curve the plane-wave calculation, and the dash-dotted curve the DWIA calculation with only the $^1S_0$ term. In each case, the $A$ amplitude is large at low energies, has a minimum near 50 MeV, and rises slightly at higher energies. The $B$ term has an inverted behavior and is comparable to the $A$ term near 50 MeV. Distortion has the effect of reducing the $A$ amplitude below 50 MeV and raising it between 50 and 80 MeV; it has an opposite effect on the $B$ term. The importance of the $B$ term is strongly enhanced near 50 MeV when only the $^1S_0$ amplitude is used, illustrating the fact that this amplitude maximizes the correlations between the two valence nucleons.

## V. SUMMARY AND CONCLUSIONS

We have presented here the most complete study of low-energy DCX cross sections now available on a single nucleus. The measurements extend to a lowest energy of 19 MeV where the 0° cross section was found to be approximately half of that at 50 MeV. The forward-angle DIAS excitation function for $^{14}C$ is now well mapped out from 19 to 300 MeV. Phenomenological isospin-dependent optical-potential calculations are shown to be capable of giving a good description of the data between 29.1 and 64.4 MeV, but require the use of an isotensor term that simulates the effects of transitions through nonanalog intermediate states or other short-range correlations.

The microscopic second-order DWIA calculations presented here account in general for the shapes of the angular distributions, but the magnitude and energy dependence of the 0° cross sections is not well reproduced. The effects of distortions, including those of the intermediate $\pi^0$, are found to be important at all energies. Contributions from a double-spin-flip term are found to increase rapidly with energy and cannot be disregarded. Pion true absorption is also found to be important, but is not well constrained by existing data.

In view of the disagreement between the microscopic DWIA calculations and the data between 30 and 60 MeV, we must conclude that important physical effects are still missing from the model. The sensitivity to the angular structure of the nuclear wave functions suggests that the solution may involve short-range correlations of the two nucleons that are not treated in the present calculations. Thus, amplitudes from the $s$-$d$ shell in an extended shell-model description of nuclear structure may provide additional correlations.[6] Alternatively, dynamical possibilities include the effects of meson-exchange terms which involve the charge-exchange scattering of the incident $\pi^+$ with a virtual $\pi^-$ from the nuclear medium.[24]

The study of exclusive DCX reactions at pion energies between 20 and 80 MeV is thus an excellent means for probing nucleon-nucleon correlations in nuclei which produce large effects in the DIAS cross sections. The discrepancies observed here between the data and the microscopic DWIA calculations require additional experimental and theoretical studies. Such investigations should enable one to determine whether pion charge-exchange reactions can be described within a conventional framework of nucleons and mesons or will require exotic degrees of freedom.

## ACKNOWLEDGMENTS

We thank the LAMPF staff for their assistance in carrying out these measurements. This work was supported in part by the U.S. Department of Energy, the National Science Foundation, and the United States–Israel Binational Science Foundation.

*Present address: Los Alamos National Laboratory, Los Alamos, NM 87545.

†Present address: TRIUMF, 4004 Wesbrook Mall, Vancouver, BC V6T 2A3 Canada.

‡Present address: Argonne National Laboratory, Argonne, IL 60439.

§Present address: University of Massachusetts, Amherst, MA 01003.

[1]E. R. Siciliano, M. D. Cooper, Mikkel B. Johnson, and M. J. Leitch, Phys. Rev. C **34**, 267 (1986).

[2]F. Irom, M. J. Leitch, H. W. Baer, J. D. Bowman, M. D. Cooper, B. J. Dropesky, E. Piasetzky, and J. N. Knudson, Phys. Rev. Lett. **55**, 1862 (1985).

[3]J. L. Ullman, P. W. F. Alons, J. J. Kraushaar, J. H. Mitchell, R. J. Peterson, R. A. Ristinen, J. N. Knudson, J. R. Comfort, H. W. Baer, J. D. Bowman, M. D. Cooper, D. H. Fitzgerald, F. Irom, M. J. Leitch, and E. Piasetzky, Phys. Rev. C **33**, 2092 (1986).

[4]T. Karapiperis and M. Kobayashi, Phys. Rev. Lett. **54**, 1230 (1985).

[5]Gerald A. Miller, Phys. Rev. Lett. **53**, 2008 (1984).

[6]W. R. Gibbs, W. B. Kaufmann, and P. B. Siegel, in *Proceedings of the LAMPF Workshop on Pion Double Charged Exchange,* edited by H. W. Baer and M. J. Leitch, Los Alamos National Laboratory Report No. LA-10550-C, 1985 (Los Alamos National Laboratory, Los Alamos, 1985), p. 90.

[7]M. Bleszynski and R. J. Glauber, Phys. Rev. C **36**, 681 (1987). Our calculation agrees in the PWIA limit quite accurately with the calculation of Bleszynski and Glauber provided that we use the same pion-nucleon amplitudes and range and use the same nuclear density. Our nuclear density, described in the text, has a larger (and we believe more realistic) rms radius than theirs. This in part accounts for our lower values of the DCX cross section at 50 MeV. We thank M. Bleszynski for discussions on these points.

[8]M. J. Leitch, E. Piasetzky, H. W. Baer, J. D. Bowman, R. L. Burman, B. J. Dropesky, P. A. M. Gram, F. Irom, D. Roberts, G. A. Rebka, Jr., J. N. Knudson, J. R. Comfort, V. A. Pinnick, D. H. Wright, and S. A. Wood, Phys. Rev. Lett. **54**, 1482 (1985).

[9]I. Navon, M. J. Leitch, D. A. Bryman, T. Numao, P. Schlatter, G. Azuelos, R. Poutissou, R. A. Burnham, M. Hasinoff, J.-M. Poutissou, J. A. Macdonald, J. E. Spuller, C. K. Hargrove, H. Mes, M. Blecher, K. Goto, M. Moinester, and H. Baer, Phys. Rev. Lett. **52**, 105 (1984).

[10]A. Altman, R. R. Johnson, U. Wienands, N. Hessey, B. M. Barnett, B. M. Forster, N. Grion, D. Mills, F. M. Rozon, G. R. Smith, R. P. Trelle, D. R. Gill, G. Sheffer, and T. Anderl, Phys. Rev. Lett. **55**, 1273 (1985); T. Anderl, thesis, Reinischen Friedrich-Wilhelms-Universität zu Bonn, 1987.

[11]Peter A. Seidl, Mark D. Brown, Rex. R. Kiziah, C. Fred Moore, Helmut Baer, C. L. Morris, G. R. Burleson, W. B. Cottingame, Steven J. Greene, L. C. Bland, R. Gilman, and H. T. Fortune, Phys. Rev. C **30**, 973 (1984); R. Gilman, H. T. Fortune, J. D. Zumbro, Peter A. Seidl, C. Fred Moore, C. L. Morris, J. A. Faucett, G. R. Burleson, S. Mordechai, and Kalvir S. Dhuga, *ibid.* **33**, 1082 (1986).

[12]R. L. Burman, R. L. Fulton, and M. Jakobson, Nucl. Instrum. Methods **131**, 29 (1975).

[13]L. G. Atencio, J. F. Amann, R. L. Boudrie, and C. L. Morris, Nucl. Instrum. Methods **187**, 381 (1981).

[14]Felix E. Obenshain, F. E. Bertrand, E. E. Gross, N. W. Hill, J. R. Wu, R. L. Burman, M. Hamm, M. J. Leitch, R. D. Edge, B. M. Preedom, M. A. Moinester, M. Blecher, and K. Gotow, Phys. Rev. C **27**, 2753 (1983); B. M. Preedom, S. H. Dam, C. W. Darden III, R. D. Edge, D. J. Malbrough, T. Marks, R. L. Burman, M. Hamm, M. A. Moinester, R. P. Redwine, M. A. Yates, F. E. Bertrand, T. P. Cleary, E. E. Gross, N. W. Hill, C. A. Ludemann, M. Blecher, K. Gotow, D. Jenkins, and F. Milder, *ibid.* **23**, 1134 (1981); M. Blecher, K. Gotow, D. Jenkins, F. Milder, F. E. Bertrand, T. P. Cleary, E. E. Gross, C. A. Ludemann, M. A. Moinester, R. L. Burman, M. Hamm, R. P. Redwine, M. Yates-Williams, S. Dam, C. W. Darden III, R. D. Edge, D. J. Malbrough, T. Marks, and B. M. Preedom, *ibid.* **20**, 1884 (1979); M. J. Leitch, R. L. Burman, R. Carlini, S. Dam, V. Sandberg, M. Blecher, K. Gotow, R. Ng, R. Auble, F. E. Bertrand, E. E. Gross, F. E. Obenshain, J. Wu, G. S. Blanpied, B. M. Preedom, B. G. Ritchie, W. Bertozzi, M. V. Hynes, M. A. Kovash, and R. P. Redwine, *ibid.* **29**, 561 (1984).

[15]S. J. Greene, D. B. Holtkamp, W. B. Cottingame, C. Fred Moore, G. R. Burleson, C. L. Morris, H. A. Thiessen, and H. T. Fortune, Phys. Rev. C **25**, 924 (1982); S. J. Greene, W. J. Braithwaite, D. B. Holtkamp, W. B. Cottingame, C. F. Moore, G. R. Burleson, G. S. Blanpied, A. J. Viescas, G. H. Daw, C. L. Morris, and H. A. Thiessen, *ibid.* **25**, 927 (1982); R. L. Burman, M. P. Baker, M. D. Cooper, R. H. Heffner, D. M. Lee, R. P. Redwine, J. E. Spencer, T. Marks, D. J. Malbrough, B. M. Preedom, R. J. Holt, and B. Zeidman, *ibid.* **17**, 1774 (1978).

[16]J. A. Faucett, M. W. Rawool, K. S. Dhuga, J. D. Zumbro, R. Gilman, H. T. Fortune, C. L. Morris, and M. A. Plum, Phys. Rev. C **35**, 1570 (1987).

[17]J. A. Carr, H. McManus, and K. Stricker-Bauer, Phys. Rev. C **25**, 952 (1982); K. Stricker, J. A. Carr, and H. McManus, *ibid.* **22**, 2043 (1980); K. Stricker, H. McManus, and J. A. Carr, *ibid.* **19**, 929 (1979).

[18]Z. Weinfeld, E. Piasetzky, H. W. Baer, R. L. Burman, M. J. Leitch, C. L. Morris, D. H. Wright, S. H. Rokni, and J. R. Comfort, Phys. Rev. C **37**, 902 (1988).

[19]W. B. Kaufmann and W. R. Gibbs, Phys. Rev. C **28**, 1286 (1983); P. B. Siegel, Ph.D. thesis, Arizona State University, 1986. The treatment of true pion absorption is discussed in K. Masutani and K. Yazaki, Phys. Lett. **104B**, 1 (1981); Nucl. Phys. **A407**, 309 (1983).

[20]P. B. Siegel and W. R. Gibbs, Phys. Rev. C **33**, 1407 (1986).

[21]D. Ashery, I. Navon, G. Azuelos, H. K. Walter, H. J. Pfeiffer, and F. W. Schlepütz, Phys. Rev. C **23**, 2173 (1981); I. Navon, D. Ashery, J. Alster, G. Azuelos, B. M. Barnett, W. Gyles, R. R. Johnson, D. R. Gill, and T. G. Masterson, *ibid.* **28**, 2548 (1983).

[22]K. Nakai, T. Kobayashi, T. Numao, T. A. Shibata, J. Chiba, and K. Masutani, Phys. Rev. Lett. **44**, 1446 (1980).

[23]We thank Dan Strottman for providing us with these wave functions.

[24]N. Auerbach, W. R. Gibbs, and E. Piasetzky, Phys. Rev. Lett. **59**, 1076 (1987); N. Auerbach, W. R. Gibbs, J. N. Ginocchio, and W. B. Kaufmann, Phys. Rev. C **38**, 1277 (1988).

[25]E. Bleszynski, M. Bleszynski, and R. J. Glauber, Phys. Rev. Lett. **60**, 1483 (1988).